Inhibition of Drug-Induced Liver Injury in Mice Using a Positively Charged Peptide That Binds DNA

Pedro E. Marques ,[1,2*] Sofie Vandendriessche,[1*] Thiago H.C. de Oliveira,[1,2] Helena Crijns,[1] Mateus E. Lopes,[4] Marfa Blanter,[1] Sara Schuermans,[1] Karen Yu,[1] Fariba Poosti,[1] Vincent Vanheule,[1] Rik Janssens,[1] Daiane Boff,[1,2] Andreas J. Kungl,[3] Gustavo B. Menezes,[4] Mauro M. Teixeira,[2**] and Paul Proost [1**]

Hepatic cell death occurs in response to diverse stimuli such as chemical and physical damage. The exposure of intracellular contents such as DNA during necrosis induces a severe inflammatory response that has yet to be fully explored therapeutically. Here, we sought means to neutralize the ability of extracellular DNA to induce deleterious tissue inflammation when drug-induced liver injury had already ensued. DNA exposure and inflammation were investigated *in vivo* in drug-induced liver injury using intravital microscopy. The necrotic DNA debris was studied in murine livers *in vivo* and in DNA debris models *in vitro* by using a positively charged chemokine-derived peptide (MIG30; CXCL9[74-103]). Acetaminophen-induced liver necrosis was associated with massive DNA accumulation, production of CXC chemokines, and neutrophil activation inside the injured tissue. The MIG30 peptide bound the healthy liver vasculature and, to a much greater extent, to DNA-rich necrotic tissue. Moreover, MIG30 bound extracellular DNA directly *in vivo* in a charge-dependent manner and independently of glycosaminoglycans and chemokines. Post-treatment of mice with MIG30 reduced mortality, liver damage, and inflammation significantly. These effects were not observed with a control peptide that does not bind DNA. Mechanistically, MIG30 inhibited the interaction between DNA and histones, and promoted the dissociation of histones from necrotic debris. MIG30 also inhibited the pro-inflammatory effect of CpG DNA, as measured by a reduction in CXCL8 production, indicating that MIG30 disturbs the ability of DNA to induce hepatic inflammation. *Conclusion:* The use of DNA-binding peptides reduces necrotic liver injury and inflammation, even at late timepoints. (*Hepatology Communications* 2021;5:1737-1754).

Necrotic cell death underlies the pathology of numerous diseases.[1] Hepatocyte necrosis is central in drug-induced liver injury, a severe medical condition that leads to most acute liver failure cases.[2,3] An immediate consequence of necrosis is the release of unprocessed intracellular contents, which will invariably initiate an intense inflammatory process in the tissue, including chemokine production and neutrophil recruitment.[4] Moreover, the persistence of necrotic debris in the tissue may aggravate the collateral inflammatory damage, while delaying liver regeneration. The release of a specific cellular component, DNA, appears to be critical to increase the inflammatory response and disease severity during acute liver injury, as shown by us and others.[5-8] Extracellular DNA released from necrotic cells is recognized by

Abbreviations: ALT, alanine aminotransferase; APAP, acetaminophen; CXCL, CXC chemokine ligand; ELISA, enzyme-linked immunosorbent assay; GAG, glycosaminoglycan; GFP, green fluorescent protein; HS, heparan sulfate; MIG30, CXCL9(74-103); MPO, myeloperoxidase; NET, neutrophil extracellular trap; PBMC, peripheral blood mononuclear cell; PBS, phosphate-buffered saline; TAMRA, 5(6)-carboxy tetramethyl rhodamine; TLR9, toll-like receptor 9; TNF-α, tumor necrosis factor alpha.

Received May 27, 2020; accepted May 11, 2021.

Additional Supporting Information may be found at onlinelibrary.wiley.com/doi/10.1002/hep4.1759/suppinfo.

**These authors contributed equally to this work.*

***These authors shared senior authorship.*

Supported by Research Foundation Flanders (FFO) (projects G0D6613N, G058421N and G0F7519M), CNPq, CAPES, KU Leuven C1 funding (C16/17/010) and the Hercules Foundation (contract AKUL/11/31); the Rega Foundation (to P.E.M., F.P., and P.P.); a postdoctoral research fellowship from FWO (to P.E.M. and F.P.); a PhD-SB fellowship from FWO (to S.V. and H.C.); a Marie Skłodowska-Curie fellowship (MSCA-IF-2018-839632 to P.E.M.); a bilateral research project from FWO and CNPq (to T.H.C.O.); a CNPq Ph.D. fellowship (40496/2018-1 to M.E.L.); the Instituto Nacional de Tecnologia (465425/2014-3); and FAPEMIG.

toll-like receptor 9 (TLR9), driving local inflammatory damage in the liver and remote injury to the lungs. However, fundamental knowledge regarding how necrotic DNA debris accumulated in the liver promotes a deleterious response is still lacking.

Here, we investigated means to inhibit the proinflammatory activity of molecules in the injured tissue, a strategy that has been used in other inflammatory conditions.[9] Chemokines are key in activating and recruiting leukocytes, and they require glycosaminoglycans (GAGs) to form gradients in the vasculature to guide leukocytes properly. Formation of chemokine gradients can be disrupted using high-affinity GAG ligands such as modified chemokines and synthetic peptides.[9] For instance, a dominant-negative CXC chemokine ligand (CXCL) 8 mutant with improved GAG-binding affinity reduces inflammation in a mouse model of antigen-induced arthritis by displacing wild-type CXCL8 from heparan sulfate GAGs.[10] Moreover, the injection of soluble GAGs[11] and oligosaccharides can also compete with chemokine binding to the endothelium, reducing leukocyte recruitment to the lungs and disease severity in a mouse model of allergic asthma.[12]

In this context, we aimed to neutralize the proinflammatory properties of necrotic DNA, to reduce the severity of liver injury. Similarly to GAGs, DNA is a long negatively charged polymer that could be targeted using the same high-affinity GAG ligands. To investigate the DNA deposits in injury sites, we used the 30–amino acid long C-terminal fragment of CXCL9 (MIG30; CXCL9[74-103]), a highly positively charged peptide that competes off chemokines bound to GAGs and reduces inflammation in the joint and peritoneum.[13,14] Using confocal intravital microscopy, we measured the release of necrotic DNA *in vivo*, the activity of recruited neutrophils, and the interaction of MIG30 with the injured liver. The binding of MIG30 to DNA debris was assessed and correlated with its potential to reduce injury and inflammation in a murine model of acute liver injury.

Materials and Methods

For an extensive description, please refer to the Supporting Materials and Methods.

MICE

C57BL/6J wild-type and LysM-eGFP ($Lyz2^{tm1.1Graf}$, C57BL/6 background) mice were from the Centro de Bioterismo at the Universidade Federal de Minas Gerais (UFMG) or the Animal Facility of the Rega Institute (KU Leuven). Animal experimentation was approved by the Animal Ethics Committee

View this article online at wileyonlinelibrary.com.
DOI 10.1002/hep4.1759

Potential conflict of interest: Nothing to report.

ARTICLE INFORMATION:

From the [1]Laboratory of Molecular Immunology, Department of Microbiology, Immunology and Transplantation, Rega Institute for Medical Research, KU Leuven, Leuven, Belgium; [2]Immunopharmacology Laboratory, Department of Biochemistry and Immunology, Universidade Federal de Minas Gerais, Belo Horizonte, Minas Gerais, Brazil; [3]Department of Pharmaceutical Chemistry, Institute of Pharmaceutical Sciences, Karl-Franzens Universität, Graz, Austria; [4]Center for Gastrointestinal Biology, Department of Morphology, Universidade Federal de Minas Gerais, Belo Horizonte, Minas Gerais, Brazil.

ADDRESS CORRESPONDENCE AND REPRINT REQUESTS TO:

Pedro E. Marques, Ph.D.
Molecular Immunology Lab, Room 06.A163
Rega Institute for Medical Research
Katholieke Universiteit Leuven–KU Leuven
Herestraat 49, Box 1042, 3000 Leuven–Belgium
E-mail: pedro.marques@kuleuven.be
Tel.: +3216327720

from UFMG (Registries 422/15 and 331/2015) and from KU Leuven (P111/2016).

LIVER INJURY MODEL

Acetaminophen (APAP; Sigma-Aldrich, St. Louis, MO) dissolved in warm saline was administered to fasted mice by oral gavage.[8] Liver injury was estimated by serum alanine aminotransferase (ALT; BioClin, Minas Gerais, Brazil) levels and histopathology of liver sections stained with hematoxylin and eosin (H&E). Liver cryo-sections were used for staining with anti-heparan sulfate (Amsbio, Abingdon, United Kingdom) and anti-Ly6G (BD Biosciences, San Jose, CA) antibodies. Myeloperoxidase (MPO) activity was measured in liver lysates. Tumor necrosis factor (TNF)-α and the chemokines CXCL1, CXCL2, and CXCL6 were quantified in liver lysates and serum samples by enzyme-linked immunosorbent assay (ELISA). For peptide treatments, mice were injected with 100 μg of unlabeled peptide 3 times, applied at timepoints 6, 12, and 18 hours after APAP overdose.

CONFOCAL INTRAVITAL MICROSCOPY

Intravital microscopy was performed as described previously.[15] Extracellular DNA was visualized by an intravenous injection of 2 μL of 5 mM Sytox green (Thermo Fisher Scientific, Waltham, MA). Neutrophils were visualized by their green fluorescent protein (GFP) signal (LysM-eGFP mice) or with a phycoerythrin-coupled anti-GR1 antibody (4 μg; BD Biosciences). MIG30-TAMRA was used at 20 μg per mouse intravenously. Imaging was performed using a Nikon C2 confocal microscope. Image analysis and neutrophil tracking were performed using Volocity (Perkin Elmer, Waltham, MA) and NIS Elements (Nikon, Tokyo, Japan).

PEPTIDES

The GAG-binding CXCL9 fragment (CXCL9[74-103]; MIG30) and a control peptide with poor GAG affinity containing only the 18 C-terminal amino acids of CXCL9 (CXCL9[86-103]) were chemically synthesized on a P11 peptide synthesizer (Activotec, Cambridge, United Kingdom), as shown previously.[13,14] Peptides were conjugated N-terminally with 5(6)-carboxy tetramethylrhodamine (TAMRA) for visualization by fluorescence.

DNA BINDING ASSAY

Ninety-six-well plates for ELISA (Corning, Corning, NY) and GAG binding plates (Galen, Chattanooga, TN) were left uncoated or were coated with 25 μg/mL of GAGs overnight. Murine CXCL6 and CXCL2 and calf thymus DNA (Sigma-Aldrich) were diluted in phosphate-buffered saline (PBS) and incubated in the plates for 2 hours. Bound DNA was detected using 1 μM Sytox green and analyzed in a Clariostar fluorimeter (BMG Labtech, Cary, NC).

BIOTINYLATED DNA BINDING ASSAY

EZ-link TFPA-PEG3-Biotin (Thermo Fisher Scientific) was used to biotinylate DNA. Ninety-six-well ELISA plates (Corning) were coated with 0.5% histones from calf thymus (Sigma-Aldrich) in PBS. After blocking with 1% bovine serum albumin (BSA), biotinylated DNA, and MIG30 were diluted in PBS and incubated in the plate for 1 hour. Wells were incubated with HRP-streptavidin and quantified by measuring converted 3,3′,5,5′-tetramethylbenzidine at 450 nm.

DNA DEPOSIT MODEL

A chambered cover glass (Labtek Inc., Grand Rapids, MI) coated with 0.1% gelatin was spotted with 10 μL of calf-thymus DNA (2 mg/mL) in PBS and allowed to dry. The precipitated DNA was stained with Sytox green (50 nM) and MIG30-TAMRA (4 μg/mL) for 10 minutes and washed 3 times with PBS. Imaging was performed on a Zeiss Axiovert 200M microscope and analyzed using FIJI.

WESTERN BLOT

HepG2 debris were stimulated with 10 μM MIG30 diluted in Hank's balanced salt solution. Supernatant was collected and proteins were run in 16% tris-glycine gels (Novex WedgeWell), transferred onto a polyvinylidene fluoride membrane and blocked with 5% BSA in trishydroxymethylaminomethane-buffered

saline Tween 20. Primary anti-histone H3 antibody (Abcam) was incubated overnight. The blot was developed with donkey anti-rabbit peroxidase antibody (Jackson ImmunoResearch Laboratories, Inc., West Grove, PA) and SuperSignal West Pico PLUS substrate (Thermo Fisher Scientific).

STATISTICAL ANALYSIS

Data were shown as mean ± SEM unless stated otherwise. *In vivo* experimental groups included a minimum of five mice and were performed at least twice. *In vitro* experiments were performed in triplicate at least twice. Comparisons between two groups were analyzed with Student *t* test and between multiple groups with one-way ANOVA. Data analysis was done using GraphPad Prism.

Results

EXTENSIVE EXTRACELLULAR DNA DEPOSITION DURING NECROTIC LIVER INJURY

To investigate the consequences of necrotic cell death in the liver, as well as the role of extracellular DNA and pro-inflammatory mediators in disease, we optimized the model of drug-induced liver injury in mice by oral APAP overdose. This is a well-established model of acute liver injury, in which hepatocytes die predominantly by necrosis.[16] Treatment of C57BL/6J mice with 600 mg/kg of APAP by oral gavage caused 40% mortality within 24 hours (Fig. 1A), indicating that this dose was sufficient to cause severe liver necrosis. Thereafter, a time-response experiment was performed to establish the peak of liver injury in mice. Using serum ALT levels as measurement of hepatocyte necrosis, we observed that mice presented significant liver damage as early as 6 hours after APAP intoxication and up to 36 hours after the overdose (Fig. 1B). Corroborating the ALT quantification, mice presented extensive hepatic necrosis, as shown by histopathology analysis of liver sections stained with H&E (Fig. 1C,D). Overall, the APAP overdose induced significant liver injury in mice, making it a robust model to investigate the immune response to necrosis.

To evaluate directly the development of liver injury and the release of DNA, we used confocal intravital microscopy, which yields a real-time observation of events happening in the tissue *in vivo*.[17] To visualize the extracellular DNA present in the injured liver, mice were injected with Sytox green, a cell-impermeable fluorescent DNA dye. Intravital imaging of APAP-treated mice revealed a massive exposure of extracellular DNA in the liver, which was absent in healthy control mice (Fig. 1E). As described previously,[6] the extracellular DNA was derived primarily from hepatocytes and found in two distinct forms: (1) DNA-rich necrotic areas: with strong Sytox staining, matching in morphology with the necrotic areas, and containing both amorphous DNA and round nuclei; (2) intravascular DNA deposits with milder Sytox staining, covering hepatic sinusoids often from the centrilobular vein to the portal triad (Fig. 1F). Evidently, an abundance of DNA is released by hepatocytes during hepatic necrosis, which has been implicated in the overt inflammatory response that contributes to the pathogenesis of necrotic liver diseases.[5-8] To evaluate the possibility that neutrophils encountering the DNA deposits would be stimulated to release neutrophil extracellular traps (NETs), we incubated purified human neutrophils with DNA (Supporting Fig. S1A-D). However, DNA was unable to induce NETosis or reactive oxygen species (ROS) production in neutrophils, indicating that it is unlikely that DNA-induced NETs are contributing to the total bulk of extracellular DNA in the liver. These observations prompted us to investigate the effects of the DNA debris on the production of pro-inflammatory mediators and leukocyte activation in the liver.

LIVER INJURY CAUSES CXC CHEMOKINE PRODUCTION AND NEUTROPHIL ACTIVATION *IN SITU*

The hepatic inflammation can be quantified by the production of cytokines and chemokines, and by the recruitment of leukocytes to the liver. As early as 6 hours after APAP overdose, significant amounts of the pro-inflammatory cytokine TNF-α and the chemokines CXCL1, CXCL2, and CXCL6 were produced in the liver (Fig. 2A-D). These mediators accumulated locally in such elevated concentrations that they were detected also in the bloodstream of APAP-treated mice. Even though several other mediators are produced during liver injury, including

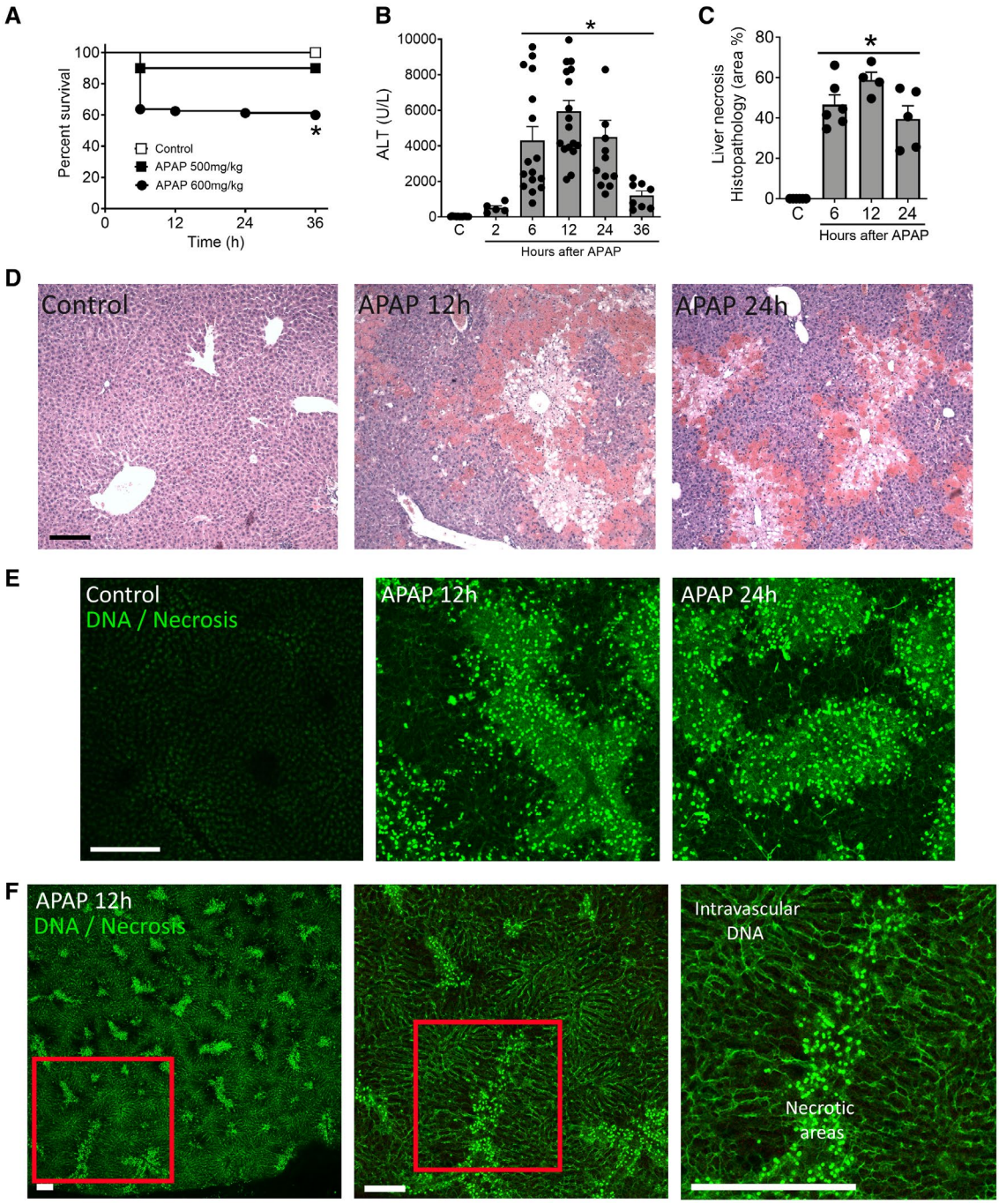

FIG. 1. Extensive extracellular DNA deposition during necrotic liver injury. (A) Survival curve of C57BL/6J mice treated with different doses of APAP by oral gavage (n ≥ 9 per group). (B) Time-course of liver injury induced by APAP (600 mg/kg), quantified by the release of ALT in the serum of mice. (C,D) Histopathological analysis of the necrotic areas in the livers of mice treated with APAP (600 mg/kg) for up to 24 hours. (E) Confocal intravital microscopy of the livers of mice treated with APAP for 12 or 24 hours. Necrotic areas exhibit a significant amount of extracellular DNA, which is evidenced by the fluorescence of Sytox green injected intravenously before imaging. (F) Intravital imaging of injured mouse livers 12 hours after APAP. Images depicted in lower to higher magnification (left to right) are the two types of DNA deposits found in the liver: intravascular DNA and necrotic areas. Data are presented as the mean ± SEM. Data were analyzed by Mantel-Cox survival test or one-way ANOVA (*$P < 0.05$). Scale bars = 100 μm.

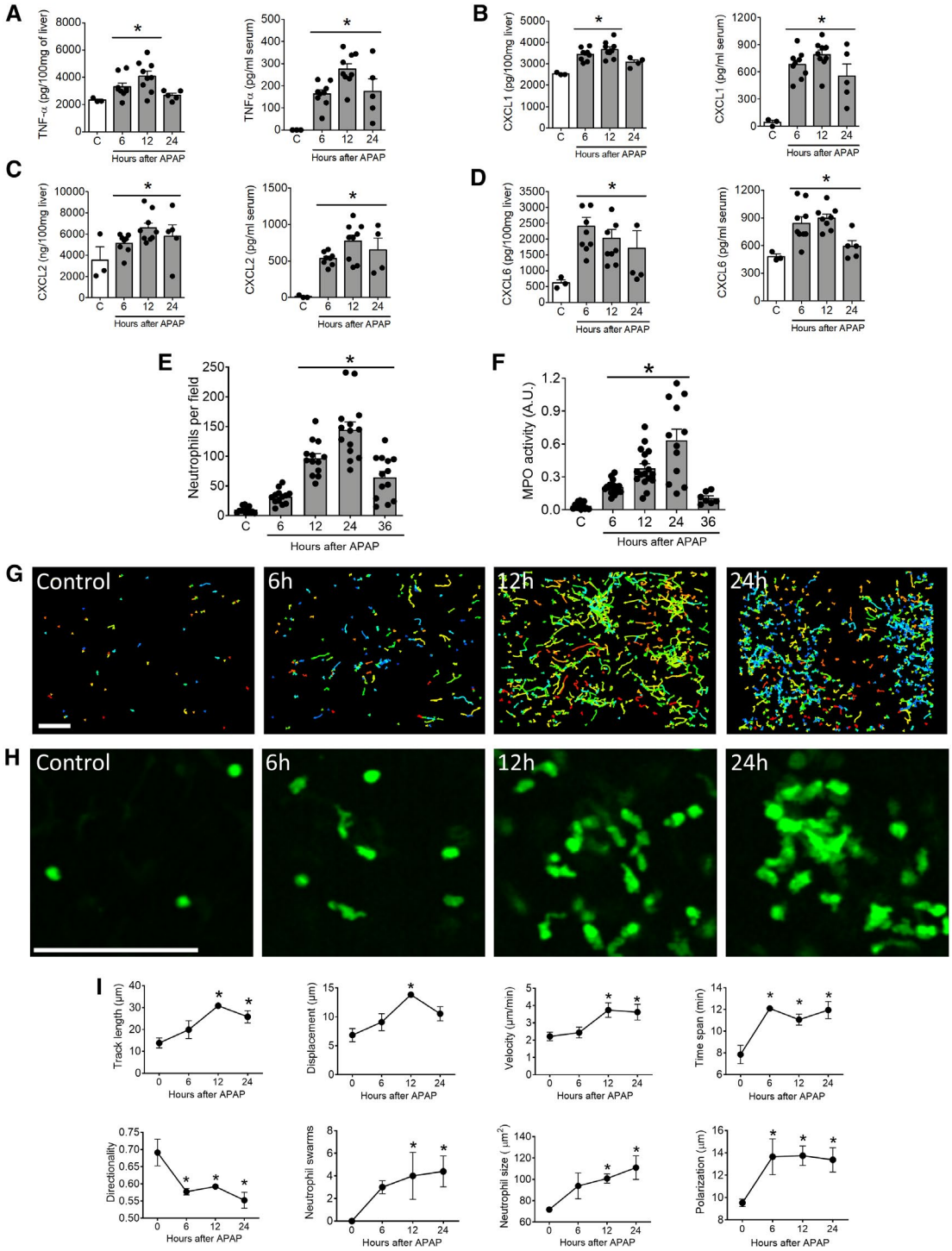

FIG. 2. Liver injury causes chemokine production and neutrophil activation. (A-D) Quantification of pro-inflammatory mediators in the liver and serum of mice treated with vehicle ("C") or APAP (600 mg/kg): TNF-α (A), CXCL1 (B), CXCL2 (C), and CXCL6 (D). (E) Neutrophil recruitment to the liver of APAP-treated mice. Neutrophils were counted by intravital microscopy in LysM-eGFP mice. (F) MPO assay estimating neutrophil infiltration in the liver of C57BL/6J mice treated with APAP. (G) Neutrophil tracking during liver injury using intravital microscopy in LysM-eGFP mice. Representative images of neutrophil tracks (rainbow colored) at each timepoint after APAP administration are shown. (H) Imaging of neutrophil activation and polarization in the inflamed liver. (I) Neutrophil movement and behavior parameters during liver injury. Data are presented as the mean ± SEM. Data were analyzed by one-way ANOVA (*$P < 0.05$). Scale bars = 100 μm.

CC chemokines and interferons,[18] it is striking that three different CXC chemokines known to be highly active neutrophil attractants were produced simultaneously. Taking that into account, we investigated the neutrophil activation state and behavior in the injured liver using intravital microscopy. Using LysM-eGFP mice, which express high levels of GFP in neutrophils,[19] we quantified the neutrophil recruitment to the liver of APAP-treated mice in the course of injury. A profound neutrophil infiltration was observed between 12 and 36 hours after injury, which was maximal at the 24-hour timepoint (Fig. 2E). This was confirmed by an MPO assay of liver lysates, which corroborated the presence of neutrophils predominantly 24 hours after APAP treatment (Fig. 2F).

A time-response evaluation of the neutrophil migration and activation during liver necrosis *in vivo* was performed, including the analysis of the movement of individual neutrophils. First, imaging of neutrophil trajectories in control mice showed these to be scarce and only migrating for short distances in the liver, as shown by the small rainbow-colored tracks (Fig. 2G). As injury developed, neutrophils became more numerous and traveled much longer distances in the liver. At the 24-hour timepoint, neutrophils had migrated specifically into the necrotic areas and were concentrated within these zones (Fig. 2G).[6] Alongside the alterations in the migration pattern, neutrophils presented significant morphological changes during liver necrosis. In control mice, neutrophils were round, as typically found in the bloodstream (Fig. 2H). However, in the injured tissue, neutrophils transitioned into ameboid, polarized cells, and formed several large clusters called neutrophil swarms.[20] The increase in polarization, in cell size (reflecting its flattening by adhesion to the substrate), and the swarming are strong indicators of neutrophil hyperactivation *in situ*, which was quantified in Fig. 2I. Interestingly, as the neutrophils started migrating longer distances (track length, displacement), moving faster (velocity), and remaining in the tissue for a longer period (time span), they lost directionality. Moreover, this happened simultaneously with the occurrence of neutrophil swarms and the increase in cell size and polarization. Altogether, it suggests that neutrophils are overwhelmingly activated by a barrage of chemoattractants in the tissue, including several CXC chemokines. This might prevent neutrophils from migrating effectively to injury sites and make them prone to damage healthy tissue.[6,8,21] In addition, it suggested that strategies to inhibit neutrophil hyperactivation could be potentially interesting, such as by disrupting the pro-inflammatory signaling by both the extracellular DNA and multiple CXC chemokine gradients in the injured liver.

MIG30, THE POSITIVELY CHARGED C-TERMINAL PEPTIDE OF A CXC CHEMOKINE, BINDS TO HEALTHY AND INJURED LIVERS

Chemokines form concentration gradients by binding to GAGs, negatively charged carbohydrates present on the endothelial surface and in tissues (Fig. 3A).[11] Chemokines are retained in place primarily through the interaction of their positively charged amino acids with GAGs, as exemplified by the binding of the C-terminus of CXCL9 to the negatively charged GAG heparan sulfate expressed by the endothelium (Fig. 3A,B). Given its strong positive charge (Fig. 3C), we hypothesized that the synthetic C-terminal fragment of CXCL9 might be used as an inhibitor of chemokine gradient formation by competing with intact chemokines for binding to endothelial GAGs. Indeed, the synthetic peptide CXCL9(74-103), or MIG30, binds avidly to GAGs and is a powerful inhibitor of leukocyte recruitment in models of acute inflammation in the joint and peritoneum.[13,14] Moreover, MIG30 could be used to investigate the abundant extracellular DNA deposits attached to the injured tissue.

The distribution and kinetics of the MIG30 peptide were evaluated in the liver of healthy and APAP-treated mice. To visualize the localization of the peptide *in vivo*, the N-terminus of MIG30 was conjugated to a fluorophore (TAMRA) and injected intravenously at a low dose (20 μg/mouse) 5 minutes before intravital imaging. In control livers, MIG30 bound to the hepatic microvasculature, which can be seen intercalating the rows of binucleated hepatocytes in the liver (Fig. 3D). However, in APAP-injured livers, MIG30 not only bound avidly to the vasculature, but also stained the DNA-rich necrotic areas extensively. In higher magnification, it was evident that MIG30 also colocalized with the intravascular DNA deposits (Fig. 3D,E). Quantification of MIG30 binding to livers by intravital microscopy showed that it binds significantly more to the injured tissue than to the livers of healthy controls (Fig. 3F).

To understand whether the interaction of MIG30 with the tissue was specific, we compared it with a fluorescently labeled poor GAG-binder control peptide consisting of the 18 C-terminal amino acids of MIG30. When injected intravenously in healthy mice, MIG30 labeled more of the hepatic vasculature and remained

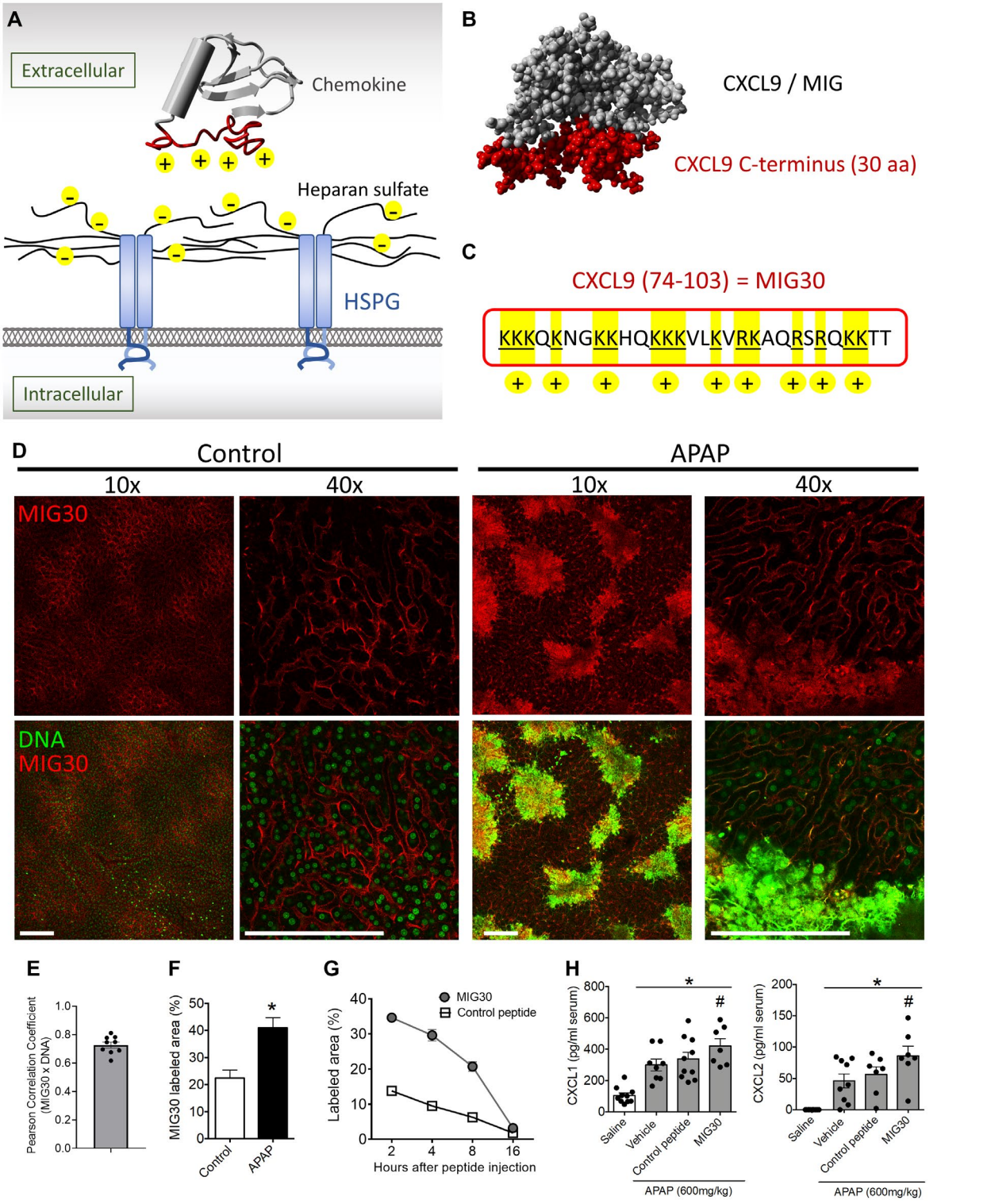

FIG. 3. MIG30, the positively charged C-terminal peptide of the chemokine CXCL9, binds to the healthy and injured liver. (A) Diagram showing the interaction between chemokines and cells. Chemokines are retained through electrostatic interactions with GAGs on the cell surface such as HS, a component of heparan sulfate proteoglycans. (B) Three-dimensional structural modeling of CXCL9, showing the C-terminus including the main GAG-binding residues in red. (C) Sequence of the MIG30 peptide (CXCL9[74-103]). Positively charged amino acids are highlighted in yellow. (D) MIG30 binds to the liver in healthy and diseased conditions. Healthy control mice or mice treated with APAP for 24 hours were injected with TAMRA-labeled MIG30 (20 μg) intravenously 5 minutes before imaging by intravital microscopy. Extracellular DNA and necrotic areas are shown by Sytox green staining. (E) Colocalization index (Pearson's correlation coefficient) between MIG30-TAMRA (20 μg) and Sytox green-stained DNA was measured in the livers of mice treated with APAP for 24 hours. (F) Liver injury induced by APAP increases MIG30 binding to the liver. (G) Evaluation of the MIG30 binding kinetics to the healthy liver in comparison to a control peptide. (H) MIG30 treatment causes the displacement of CXCL1 and CXCL2 into the bloodstream of APAP-treated mice. Data are presented as the mean ± SEM. Data were analyzed by one-way ANOVA (*$P < 0.05$). Scale bars = 100 μm. Abbreviation: HSPG, heparan sulfate proteoglycans.

bound to the liver longer than the control peptide (Fig. 3G). MIG30 binding was also compared with the binding of a fluorescently tagged isotype immunoglobulin G (IgG) antibody to the liver (Supporting Fig. S2). Isotype IgG was essentially inert to the DNA deposits and necrotic areas, binding almost exclusively to discrete spots corresponding to leukocytes and endothelial cells expressing high-affinity Fcγ receptors. Finally, MIG30 was tested functionally for its ability to disrupt chemokine binding to the tissue. We observed that APAP-injured mice treated with MIG30 (100 μg/mouse) had significantly more CXCL1 and CXCL2 in the serum in comparison with untreated or control peptide-treated animals (Fig. 3H). Importantly, the increases in serum levels of CXCL1 and CXCL2 are not due to induction of chemokine production by MIG30, as incubation of human peripheral blood mononuclear cells (PBMCs) with the peptide is unable to induce nuclear factor kappa B activation nor CXCL8 production *in vitro* (Supporting Fig. S3A,B). Endothelial cells were also insensitive to MIG30 incubation (Supporting Fig. S3C). Moreover, the MIG30 peptide does not induce NETosis or ROS production (Supporting Fig. S1A-D), showing that it does not possess direct bioactive effects on cells. These are indicative that MIG30 is indeed able to displace chemokines from the inflamed liver and endothelial surfaces, releasing them into the bloodstream.

TREATMENT WITH MIG30 RESCUES MICE FROM LIVER INJURY

Although APAP-induced liver injury and inflammation are known to be inhibited with N-acetylcysteine, this reducing agent is effective only if given soon after the APAP challenge or as a pretreatment.[22,23] Considering the lack of late treatments for drug-induced liver injury and aiming to establish the therapeutic potential of MIG30, we subjected mice to APAP-induced liver injury and post-treated these with three doses of 100 μg of MIG30, given intravenously at 6, 12, and 18 hours after the overdose, when liver damage was already evident (Fig. 1). Treatment with the peptide reduced mortality significantly (Fig. 4A), which was substantiated by significant decreases in liver injury (ALT level), neutrophil infiltration, and hepatic MPO activity (Fig. 4B-D). Mice post-treated with equal doses of the 18-amino acid control peptide were not protected against liver injury nor inflammation. Moreover, intravital imaging showed a large amount of extracellular DNA deposition in the liver of untreated mice and in animals treated with the control peptide, but it was considerably reduced in mice treated with MIG30 (Fig. 4E,F).

The activation state of neutrophils in MIG30-treated mice was also investigated. At the 24-hour timepoint, the neutrophils displayed a significantly enhanced directionality in the presence of MIG30 (Fig. 4G), which was accompanied by a reduction in neutrophil size and polarization, showing that the peptide is able to prevent excessive neutrophil activation *in situ*. Interestingly, although less activated and found in lower numbers, the neutrophils that managed to be recruited to the necrotic liver in the presence of MIG30 still migrated normally in the organ, as shown by unaltered track length, displacement, velocity, time span and swarming, indicating that MIG30 did not affect basic neutrophil motility (Supporting Fig. S4). Also, we investigated whether the neutrophil-derived protease elastase played a role in the severity of liver injury. However, treatment of APAP-challenged mice with two elastase inhibitors, sivelestat or elastase inhibitor II, did not alter the ALT levels in comparison with untreated controls (Supporting Fig. S1E).

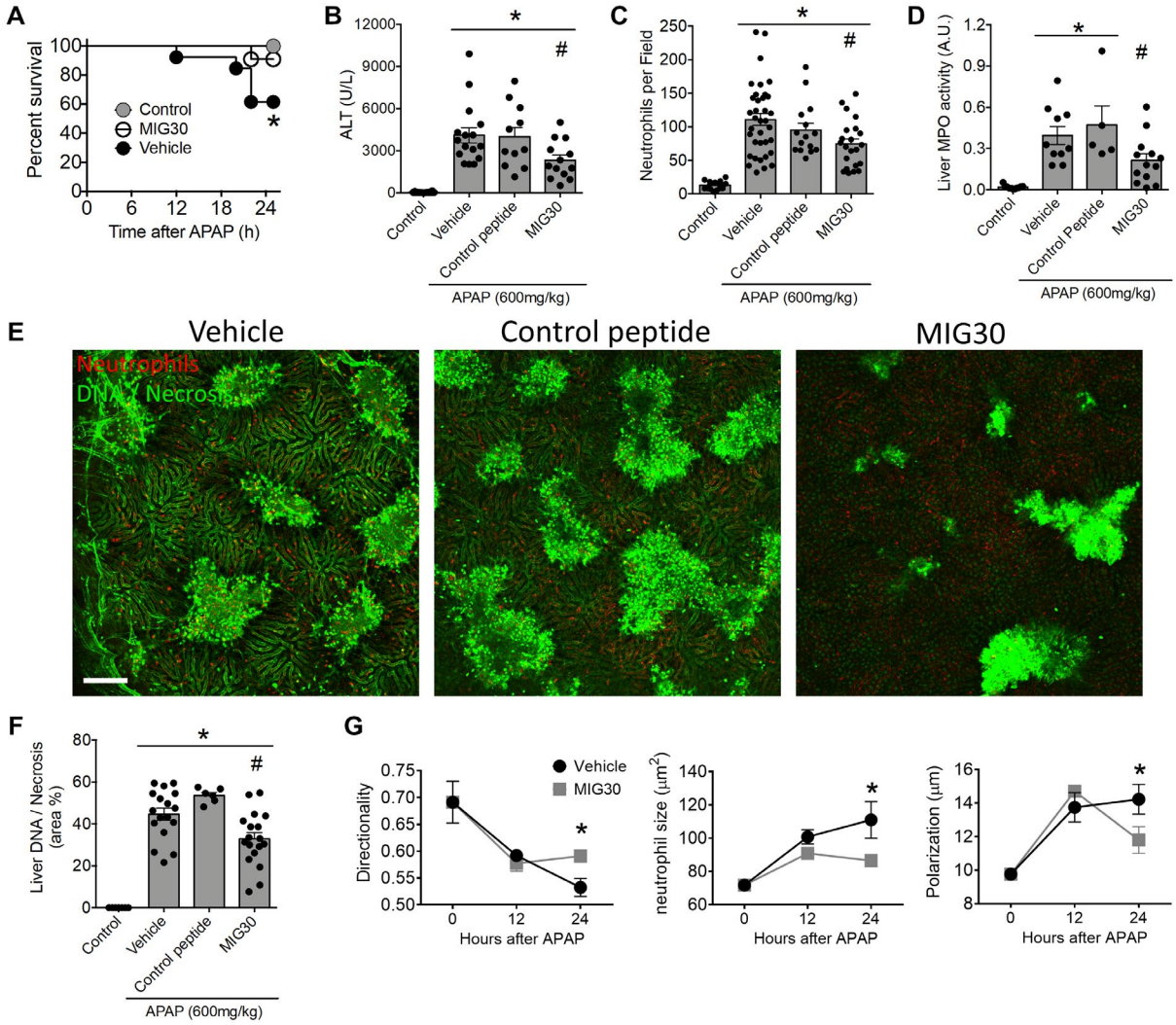

FIG. 4. Posttreatment with MIG30 rescues mice from drug-induced liver injury. (A) Survival curve of C57BL/6J mice challenged with APAP (600 mg/kg) for 24 hours and treated with MIG30. The peptide was injected intravenously in mice at 100 μg/dose, 6, 12, and 18 hours after APAP administration. (B) Reduced liver injury quantified by serum ALT levels in mice treated with MIG30 but not with control peptide. (C) Neutrophil recruitment to the liver assessed by intravital microscopy in LysM-eGFP mice. (D) MPO activity in the liver of mice challenged with APAP and treated with MIG30 or control peptide. (E) Representative intravital microscopy images of the liver of mice challenged with APAP alone (vehicle) or treated with control peptide or MIG30. Areas of extracellular DNA/necrosis are shown by Sytox green and neutrophils by an anti-GR1 antibody (red). (F) Quantification of extracellular DNA/necrosis in the liver by intravital microscopy. (G) Analysis of neutrophil directionality, size, and polarization in the liver of mice treated with APAP alone (vehicle) or with MIG30. Data are presented as the mean ± SEM. Data were analyzed by Student *t* test and one-way ANOVA. *Statistical difference ($P < 0.05$) between control and vehicle groups. #Statistical difference between vehicle and MIG30 groups. Scale bars = 100 μm.

Altogether, the MIG30 peptide was able to rescue mice from liver damage and inflammation even at a late stage, stressing its potential as a therapeutic tool for liver injury. Nevertheless, the reduction in extracellular DNA in the liver of MIG30-treated mice (Fig. 4E,F) suggested that the peptide may have acted through an unanticipated mechanism.

MIG30 BINDS TO EXTRACELLULAR DNA IN THE INJURED LIVER

Trying to elucidate the mechanisms behind the beneficial effects of MIG30 during liver injury, we decided to evaluate whether the peptide bound the extracellular DNA deposits directly *in vivo*.

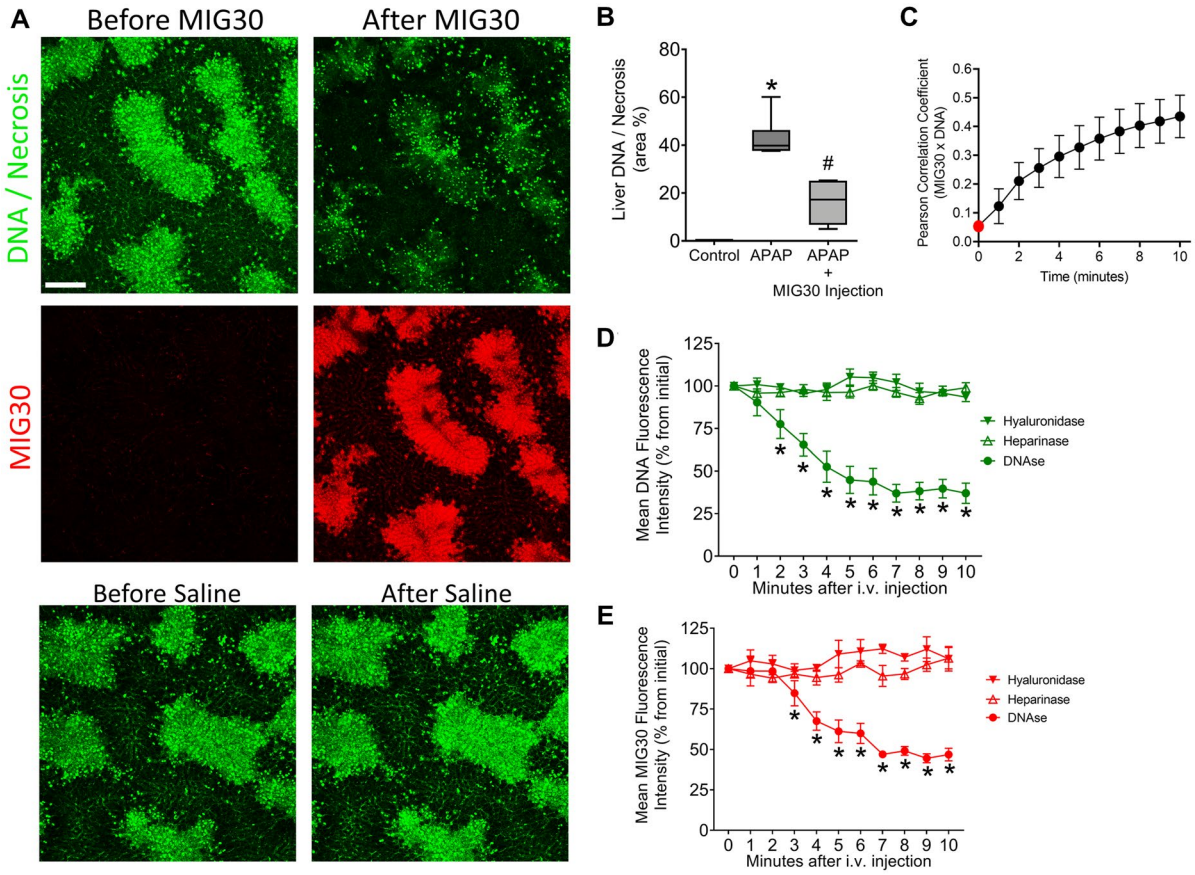

FIG. 5. MIG30 binds to extracellular DNA in the injured liver. (A) Intravital imaging of an injured murine liver (APAP 600 mg/kg, 24 hours) before (left panels) and after (right panels) an intravenous injection of 100 μg TAMRA-labeled MIG30. The extracellular DNA staining present in the liver (Sytox green) was reduced within 5 minutes (right panels) as MIG30 bound the necrotic DNA. The injection of saline (bottom panels) had no effect on the DNA exposed in the liver in the same interval. (B) Quantification of extracellular DNA fluorescence 5 minutes after an intravenous injection of 100 μg MIG30-TAMRA. (C) Colocalization index (Pearson's correlation coefficient) of MIG30 and DNA (Sytox green) in injured mice injected at time zero (red dot) with 100 μg of MIG30-TAMRA. (D,E) Mean fluorescence intensity of DNA (D; green) and MIG30 (E; red) staining in the liver of APAP-treated mice after intravenous injections of DNAse 1 (1,000 U), heparinase III (100 μg), or hyaluronidase (1,000 U). Mice received Sytox green and 20 μg of MIG30-TAMRA intravenously before the injections, and the fluorescence was measured for up to 10 minutes. Data are presented as the mean ± SD. Data were analyzed by Student *t* test and two-way ANOVA. *Statistical difference ($P < 0.05$) between control and APAP groups. #Statistical difference between APAP and MIG30 groups. Scale bars = 100 μm.

Interestingly, binding to DNA can be quantified by measuring the loss of fluorescence of DNA-intercalating dyes, which are displaced from the double-helix by distortions caused by protein binding[24] (Supporting Fig. S5). Hence, we induced necrosis and DNA deposition in the liver using the APAP-toxicity model (24 hours) and injected the injured mice intravenously with 100 μg of TAMRA-labeled MIG30. Within 5 minutes, MIG30 bound avidly to the injured hepatic tissue and reduced by 50% the extracellular DNA fluorescence in the liver (Fig. 5A-C). Importantly, the DNA fluorescence was unaltered by a bolus injection of vehicle (sterile 0.9% NaCl), showing that the effect is not due to the injection nor a change in blood volume. These data show the ability of the MIG30 peptide to bind directly to extracellular DNA exposed in the injured liver.

Furthermore, we investigated whether MIG30 could be displaced from the liver by removing the extracellular DNA. APAP-treated mice were injected with MIG30-TAMRA for staining (20 μg/mouse) and were subsequently injected intravenously with

1,000 units of the nuclease DNAse 1 for 10 minutes (Fig. 5D,E). The DNAse treatment degraded in 5 minutes approximately 50% of the extracellular DNA (Fig. 5D), and by doing so, also reduced by half the MIG30 staining in the liver (Fig. 5E). These data show that extracellular DNA and MIG30 are tightly connected and share each other's distribution *in vivo*. To further understand the binding partners of DNA and MIG30 within the necrotic tissue, we injected APAP-treated mice with hyaluronidase or heparinase to degrade the GAGs hyaluronic acid and heparan sulfate, respectively (Fig. 5D,E). Neither the DNA nor the MIG30 staining were significantly removed from the liver following injection with the glycosidases, in sharp contrast to the DNAse injection. This indicates that neither the DNA nor MIG30 are bound to GAGs in the injured liver.

THE MIG30 PEPTIDE INTERACTS WITH DNA IN A CHARGE-DEPENDENT MANNER

Considering the reciprocity between DNA and MIG30 in the necrotic tissue, we hypothesized that MIG30 bound DNA through a strong electrostatic interaction. To determine this, a model of a DNA deposit *in vitro* was devised. Briefly, a small drop of a DNA solution was applied on cover glass and dried, causing the DNA to precipitate. This purified DNA deposit was stained with the fluorescent dye Sytox green and the TAMRA-labeled MIG30 peptide (Fig. 6A). Co-staining of the DNA spot with Sytox green and MIG30 allowed us to observe that MIG30 binding was restricted to the DNA deposit (Fig. 6B). Degradation of the DNA spot by addition of DNAse 1 to the medium, as seen by the loss of the Sytox green signal, was accompanied by the simultaneous disappearance of the MIG30 signal (Fig. 6B,C), confirming that MIG30 was bound to the DNA directly.

Next, we aimed to determine the mechanism behind the MIG30–DNA interaction. It is noteworthy that both MIG30 and DNA are highly charged molecules, in which MIG30 is positively charged and DNA is negatively charged. Therefore, we assessed whether MIG30 was still able to bind DNA when the global electrostatic charges were neutralized by using increasing concentrations of NaCl. Neutralization of the electrostatic charges by an excess of NaCl inhibited the binding of MIG30 to DNA in a dose-dependent manner (Fig. 6D,E). Moreover, the increasing amount of salt did not interfere with the DNA deposit itself, only with MIG30 binding. These data indicate that the interaction between MIG30 and DNA is direct and charge-dependent. To estimate the avidity of MIG30 binding to DNA, the quantification of the loss of fluorescence of DNA-intercalating dyes was used[24] (Supporting Fig. S5). Using this strategy, we were able to estimate the half-maximum effective concentration (EC50) for MIG30 binding to DNA to be 400 nM (Fig. 6F). In contrast to MIG30, the control peptide was unable to bind to DNA. This suggests that the beneficial effect of MIG30 is connected to its ability to bind avidly to DNA.

MIG30 INTERFERES WITH THE INTERACTION BETWEEN DNA AND HISTONES IN NECROTIC DEBRIS AND INHIBITS THE PRODUCTION OF CXCL8 INDUCED BY CpG DNA

Considering the abundance of GAGs in the liver and the ability of MIG30 to bind both GAGs and DNA, we decided to investigate whether DNA debris could be bound to GAGs in necrotic areas. Staining of heparan sulfate (HS) in healthy and necrotic liver cryo-sections showed that HS was expressed by the liver sinusoidal vasculature in steady state and during disease. However, HS was lost inside necrotic areas where the highest amount of DNA (and MIG30) accumulated during injury (Fig. 7A). The absence of HS at necrotic sites corroborates our previous data (Fig. 5D,E) that negatively charged GAGs such as HS are not required to anchor DNA debris at necrotic sites. The lack of a role for GAGs was further confirmed *in vitro* by developing a DNA binding test on 96-well plates, either uncoated or coated with different GAGs. Incubation of uncoated wells with increasing concentrations of DNA suffices to allow binding of DNA to plates (Fig. 7B), as GAG-binding plates have an enhanced positive surface charge at physiological pH.[25] Interestingly, the binding of DNA to the plates was dependent only on the concentration of the nucleic acid, and therefore completely independent of the GAG type the wells were coated with (Fig. 7B). This illustrates that the intrinsic electrostatic charges

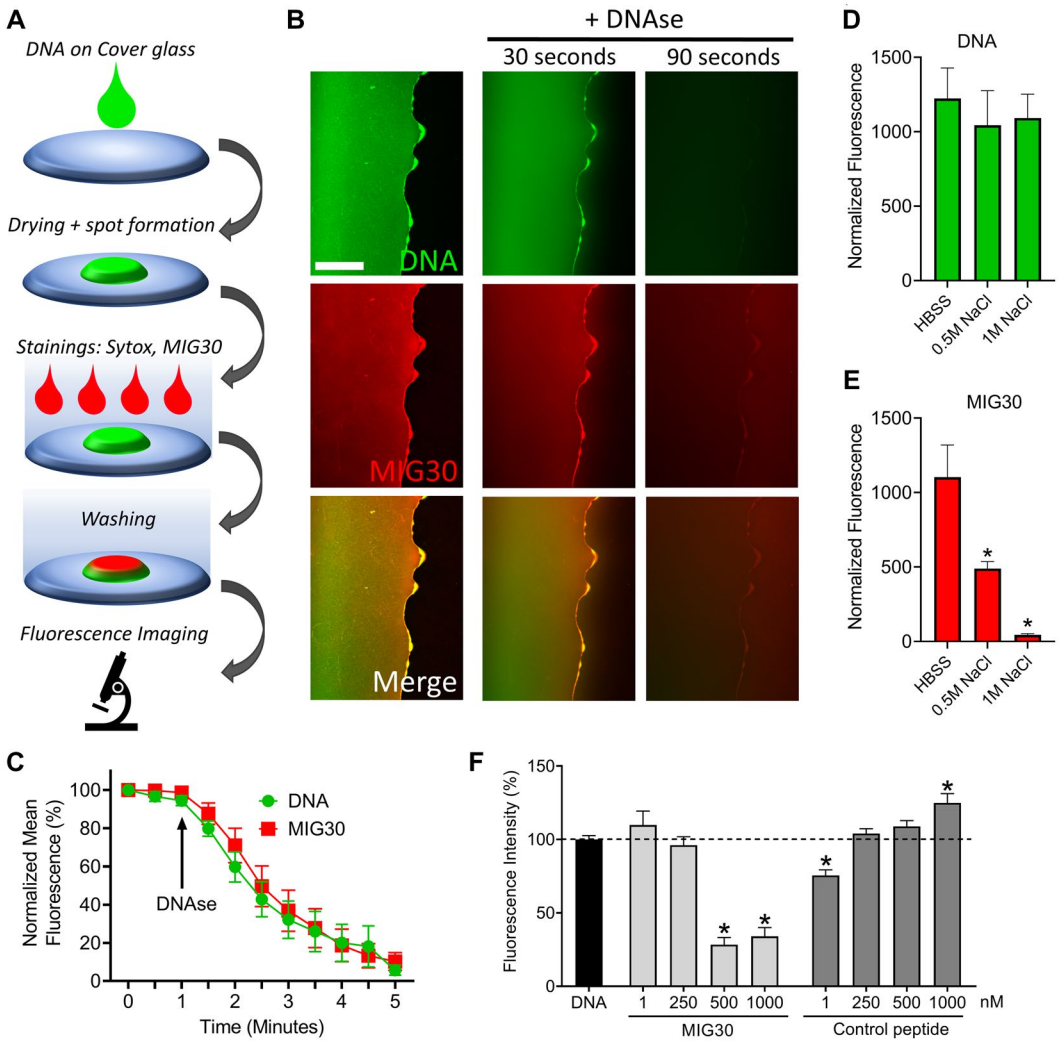

FIG. 6. The MIG30 peptide interacts with DNA directly in a charge-dependent manner. (A) Diagram of the DNA deposit model *in vitro* to study the interaction of peptides with purified DNA on coverslips. (B) Staining of DNA spots with Sytox green and MIG30-TAMRA. Both fluorescent reagents co-localize on the DNA spot and are simultaneously eliminated following treatment with DNAse. (C) Quantification of the fluorescence intensity of Sytox green and MIG30-TAMRA on DNA spots during treatment with DNAse. (D,E) Staining of DNA by MIG30 requires electrostatic interactions. The charges on DNA and MIG30 were neutralized using an excess of sodium chloride (0.5-1 M). (F) Quantification of MIG30 and control peptide binding to DNA. The fluorescence intensity of Sytox green was measured in wells that were coated with 50 μg/mL DNA, to which increasing concentrations of MIG30 and control peptide (CXCL9[86-103]) were added. Data are presented as the mean ± SEM. Data were analyzed by one-way ANOVA (*P < 0.05). Scale bars = 100 μm.

of DNA are sufficient to promote its interaction with substrates and that GAGs do not improve DNA binding.

To assess whether the abundance of chemokines in the liver (Fig. 2A-D) was acting as a bridging agent for DNA, we investigated whether GAGs and chemokines were jointly required for DNA binding to surfaces, as these two molecules are closely associated *in vivo*. GAG plates were coated with HS or hyaluronic acid, and further incubated with two CXC chemokines found in the injured liver, murine CXCL6 and CXCL2, before adding DNA to the wells. Interestingly, the type of GAG or presence of chemokines did not improve DNA binding, which was similar independently of the molecules used (Fig. 7C,D). Moreover, MIG30 bound to DNA in the

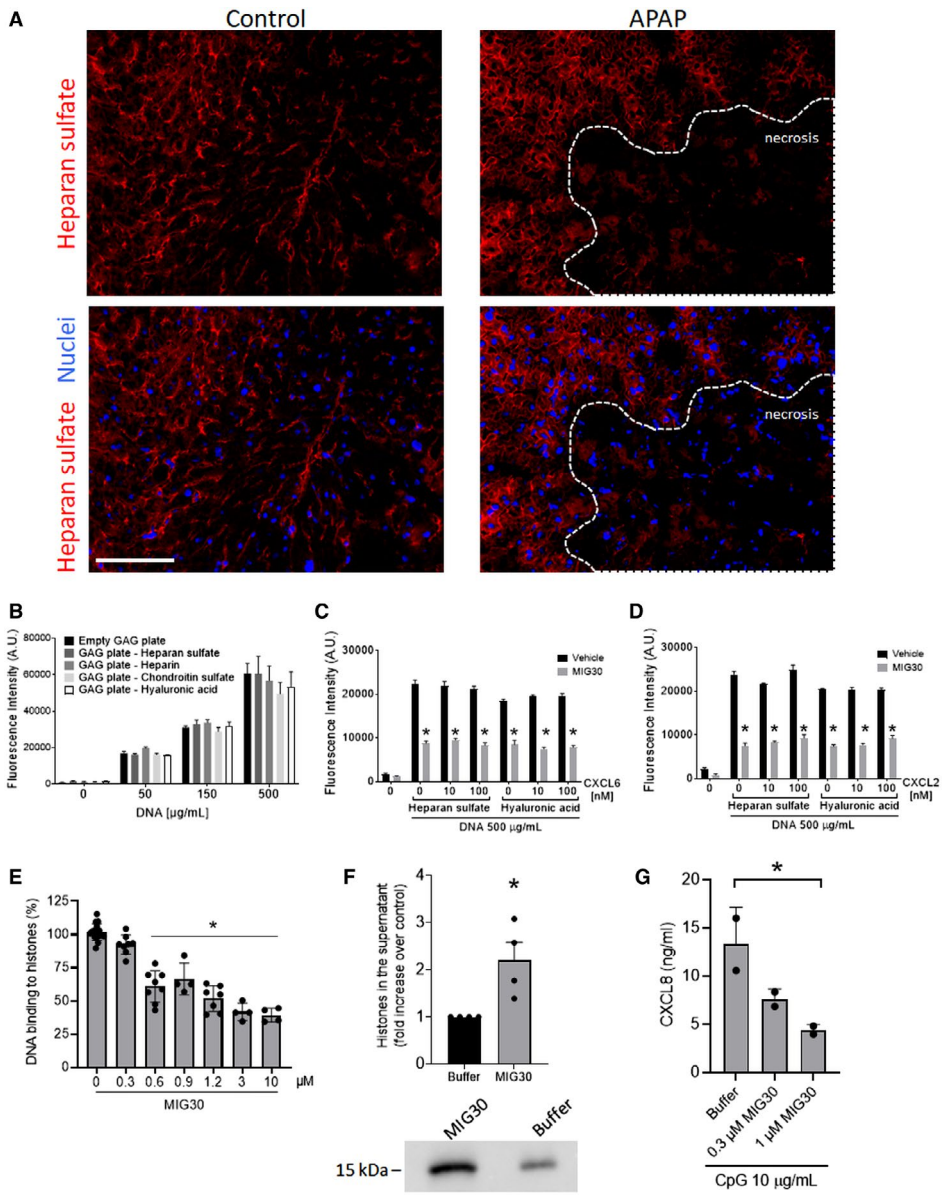

FIG. 7. MIG30 interferes with the interaction between DNA and histones in necrotic debris and inhibits the production of CXCL8 induced by CpG DNA. (A) Immunostaining of HS in liver cryo-sections of vehicle (control) or APAP-treated mice. HS is shown in red, and Hoechst-stained nuclei in blue. (B) *In vitro* DNA binding assay in the absence or presence of different GAGs. DNA binding to GAG plates was detected using Sytox green and measured in a fluorimeter. (C,D) DNA binding to GAG plates coated with HS or hyaluronic acid and co-incubated with the chemokines CXCL6 (C) or CXCL2 (D). The MIG30 peptide was used at 1 µM. (E) Quantification of biotinylated DNA binding to histones in the presence of increasing MIG30 concentrations. (F) Western blotting for histone H3 in supernatant of HepG2 debris incubated with MIG30. (G) Quantification of CXCL8 in the supernatant of PBMCs stimulated with 10 µg/mL CpG DNA and co-incubated with 0.3-1.0 µM MIG30. Data are presented as the mean ± SEM. Data were analyzed by one-way ANOVA or *t* test (**P* < 0.05). Scale bars = 100 µm.
[Correction added on september 13, 2021 after first online publication: The figure has been updated to include Panel G.]

same extent independently of the GAG or chemokine in the well. These data support the notion that GAGs and chemokines are not associated to extracellular DNA in the injured liver, and that MIG30 is not interfering with DNA interactions with these molecules.

Considering the avidity of MIG30 toward DNA, we hypothesized that MIG30 was inhibiting the

interaction of DNA with other proteins. To evaluate this, the binding of DNA to histones was quantified in the presence of increasing concentrations of MIG30. To avoid the interference of MIG30 in DNA fluorescence, we used biotinylated DNA and measured the binding of DNA to histones using a streptavidin peroxidase–based assay. Interestingly, MIG30 inhibited the binding of DNA to histones in a dose-dependent manner, with an approximate EC50 of 1.2 μM (Fig. 7E). This effect was further investigated by evaluating whether MIG30 could dissociate histones from DNA in necrotic cells. For such, necrotic cell debris were generated *in vitro* by mechanical disruption of HepG2 cells and the debris were collected for incubation with the peptide. Treatment of necrotic debris with MIG30 increased the amount of histones displaced into the supernatant significantly, as compared with buffer alone (Fig. 7F). These data indicate that MIG30 can dissociate the interaction between DNA and histones in necrotic debris, which may inhibit its pro-inflammatory properties and predispose the extracellular DNA to degradation *in vivo*. In line with this, in addition to genomic DNA, mitochondrial DNA is also released during liver necrosis. Mitochondrial DNA contains unmethylated CpG motifs and acts as a major inflammatory stimulus through TLR9 activation. To evaluate whether MIG30 might affect this pathway, freshly isolated PBMCs were stimulated with CpG DNA and co-incubated with MIG30, where after CXCL8 production was quantified in the supernatant. We observed that MIG30 was able to reduce significantly the production of CXCL8 induced by CpG in a dose-dependent manner (Fig. 7G). This indicates that MIG30 may reduce the inflammation and neutrophil activation observed in the injured liver by neutralizing the stimulatory properties of mitochondrial DNA. Altogether, the data suggest that MIG30 reduces the severity of APAP-induced liver injury by binding to DNA and interfering with its association to histones and capacity to promote inflammation.

Discussion

In this study, we investigated the means to inhibit the contribution of extracellular DNA to the severity of drug-induced liver injury. We found that MIG30, a positively charged peptide, is able to reduce liver injury and inflammation significantly by binding avidly to extracellular DNA and disrupting its interaction with histones and pro-inflammatory properties (Fig. 8). Interestingly, MIG30 was effective even if given at a late timepoint (i.e., 6 hours after the APAP challenge). These results are supported by a previous study showing that DNAse posttreatment is similarly protective against APAP-induced liver injury, by reducing DNA accumulation in the inflamed liver.[6]

It was recently shown that the polybasic sequences in histone tails are recognized by the receptor Clec2d in macrophages.[26] Clec2d is not a signaling receptor *per se*, but it carries histone-bound DNA to the endosomal compartment where it activates TLR9, triggering inflammation. Interestingly, the polybasic sequences recognized by Clec2d have a strikingly similar number of positive residues and peptide length to MIG30. Thus, one may speculate that MIG30 could be reducing liver inflammation by inhibiting nucleosome binding to Clec2d and by dissociating the histone carrier from DNA.

Liver necrosis is not the only condition in which extracellular DNA plays a role. NETs have been found in numerous tissues and diseases, and their pathological role often derives from the DNA scaffold generated during NETosis.[27] Our data indicate that the MIG30 peptide disrupts the deleterious effects of extracellular DNA *in vivo*, which may be especially useful in conditions of broad NET release such as sepsis and vasculitis.[28] It is important to mention that the extracellular DNA found in the liver is likely not from NETs. Besides the fact that hepatocytes are the main target of APAP toxicity and a plentiful source of DNA, the extracellular deposits were already present before maximal neutrophil recruitment to the liver (Figs. 1 and 2), they were found negative for neutrophil elastase staining, and occurred even when neutrophil recruitment was significantly inhibited by treatment with an anti-CXCR2 antibody.[6] Moreover, inhibition of elastase in APAP-injured mice yielded no protection (Supporting Fig. S1E), further supporting the notion that NETs were not being deployed during liver injury.

Although a surprising effect, the binding of MIG30 to DNA is not unexpected due to their complementary electrostatic charges. An immediate advantage of

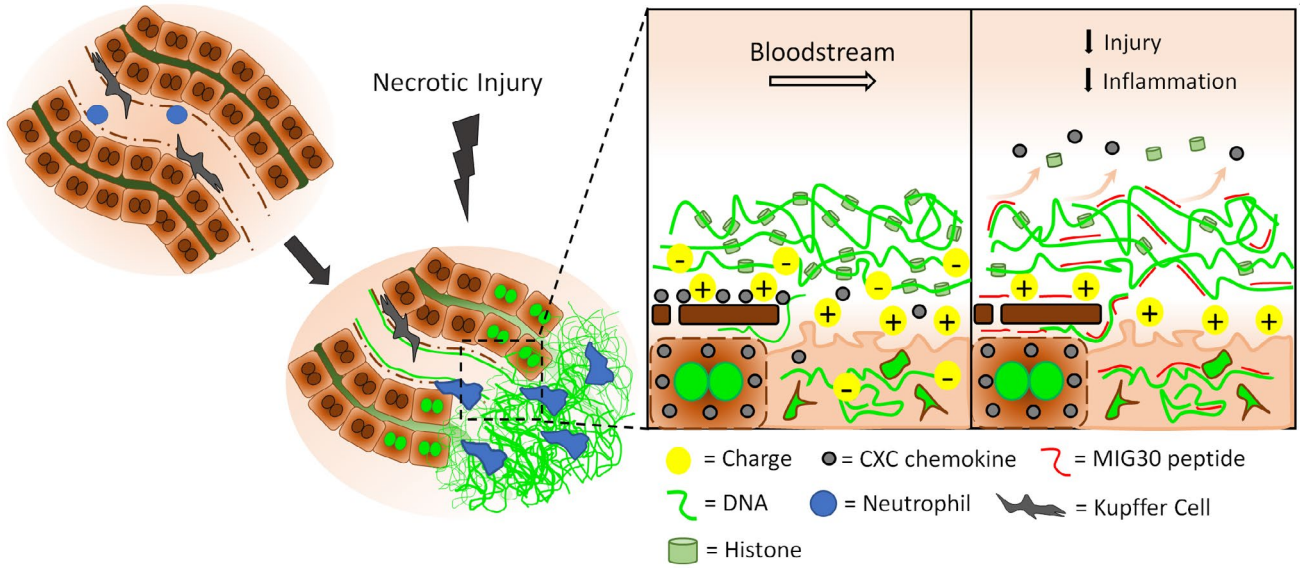

FIG. 8. Working model of MIG30 binding to extracellular DNA in liver injury sites.

that interaction is that MIG30 is an excellent probe for extracellular DNA and necrosis both *in vivo* and *in vitro* (Figs. 3 and 6). The strong positive charge of MIG30 was a requirement for DNA binding and was involved in its ability to inhibit DNA-histone binding (Figs. 6 and 7). Nonetheless, the exact motif in the peptide that is responsible for a higher affinity to DNA remains to be investigated. We hypothesize that a GAG-binding domain or the particular spacing of positively charged residues may contribute to the effects of MIG30.

Tissue necrosis is a powerful inducer of neutrophil activation and recruitment. Out of the myriad of molecules released during injury, formyl-peptides, LTB4, and CXC chemokines were consistently implicated in neutrophil chemotaxis and activation.[20,29] The fact that neutrophils migrate more and faster, concomitantly to losing directionality (Fig. 2I), suggests that these cells are "overwhelmed" by multiple chemotactic cues. In this sense, the advantage of MIG30 would be to neutralize multiple pro-inflammatory mediators (DNA and CXC chemokines) simultaneously, reducing neutrophil hyperactivation (Fig. 4G) without the deleterious effect of immunosuppression. It is important to highlight that neutrophil recruitment to injured tissues acts as a double-edged sword. Although damaging in early phases of injury and inflammation, the activity of neutrophils is required for both regeneration and tissue repair. The ability of neutrophils to amplify injury has been demonstrated in multiple experiments, such as by reducing the ALT levels and mortality in mice that were depleted of neutrophils using a neutralizing antibody,[21] by reducing liver injury after APAP when neutrophil chemotactic receptors CXCR2 and FPR1 are inhibited,[8] and by worsening liver injury when APAP-challenged mice receive an adoptive transfer of TLR9-expressing neutrophils.[6] This is an unavoidable cost of the participation of neutrophils in tissue recovery, in which they were shown to drive debris clearance from injury sites, allowing tissue regeneration, and to provide matrix metalloproteases that contribute to liver repair.[29,30] Therefore, the apparent controversial role of neutrophils remains in the field, and the development of molecules that may dissect the undesired consequences of neutrophil activation from their necessary role in tissue repair would be very valuable.

In addition to guiding neutrophil migration, CXC chemokines were also shown to stimulate liver regeneration.[31,32] Treatment with MIG30 caused an increase in the serum levels of CXCL1 and CXCL2 in mice challenged with APAP, probably by displacing chemokines from the inflamed hepatic endothelium into the bloodstream (Fig. 3H). The increased availability of chemokines in the bloodstream of MIG30-treated mice may improve liver regeneration, as observed in mice injected with CXC chemokines intravenously

in a similar model.[31] Thus, the release of chemokines from endothelial GAGs may have a dual effect: It destroys the neutrophil-guiding gradient while releasing chemokines to stimulate hepatocyte proliferation and liver regeneration. Moreover, the binding of MIG30, a chemokine fragment, to DNA suggests that full-length CXCL9 may bind DNA similarly. Interestingly, it was shown recently that the chemokines CXCL9, CXCL10, and CXCL11 bind to bacterial DNA present in skin injury, and it drives a type-I interferon response that stimulates wound healing.[33]

In summary, we found that a small positively charged peptide, MIG30, reduced liver injury after APAP overdose even at a late stage by binding avidly to DNA, inhibiting its interaction with histones and restraining neutrophil activation and inflammation in the necrotic liver.

REFERENCES

1) **Vanden Berghe T**, **Linkermann A**, Jouan-Lanhouet S, Walczak H, Vandenabeele P. Regulated necrosis: the expanding network of non-apoptotic cell death pathways. Nat Rev Mol Cell Biol 2014;15:135-147.
2) Stravitz RT, Lee WM. Acute liver failure. Lancet 2019;394:869-881.
3) European Association for the Study of the Liver. ASL Clinical Practice Guidelines: drug-induced liver injury. J Hepatol 2019;70:1222-1261.
4) Westman J, Grinstein S, Marques PE. Phagocytosis of necrotic debris at sites of injury and inflammation. Front Immunol 2019;10:3030.
5) Imaeda AB, Watanabe A, Sohail MA, Mahmood S, Mohamadnejad M, Sutterwala FS, et al. Acetaminophen-induced hepatotoxicity in mice is dependent on Tlr9 and the Nalp3 inflammasome. J Clin Invest 2009;119:305-314.
6) **Marques PE**, **Oliveira AG**, Pereira RV, David BA, Gomides LF, Saraiva AM, et al. Hepatic DNA deposition drives drug-induced liver injury and inflammation in mice. Hepatology 2015;61:348-360.
7) McGill MR, Sharpe MR, Williams CD, Taha M, Curry SC, Jaeschke H. The mechanism underlying acetaminophen-induced hepatotoxicity in humans and mice involves mitochondrial damage and nuclear DNA fragmentation. J Clin Invest 2012;122:1574-1583.
8) Marques PE, Amaral SS, Pires DA, Nogueira LL, Soriani FM, Lima BHF, et al. Chemokines and mitochondrial products activate neutrophils to amplify organ injury during mouse acute liver failure. Hepatology 2012;56:1971-1982.
9) Proudfoot AEI, Johnson Z, Bonvin P, Handel TM. Glycosaminoglycan interactions with chemokines add complexity to a complex system. Pharmaceuticals (Basel) 2017;10:70.
10) Falsone A, Wabitsch V, Geretti E, Potzinger H, Gerlza T, Robinson J, et al. Designing CXCL8-based decoy proteins with strong anti-inflammatory activity in vivo. Biosci Rep 2013;33:e00068.
11) Kuschert GS, Coulin F, Power CA, Proudfoot AE, Hubbard RE, Hoogewerf AJ, et al. Glycosaminoglycans interact selectively with chemokines and modulate receptor binding and cellular responses. Biochemistry 1999;38:12959-12968.
12) **Nonaka M**, **Bao X**, Matsumura F, Gotze S, Kandasamy J, Kononov A, et al. Synthetic di-sulfated iduronic acid attenuates asthmatic response by blocking T-cell recruitment to inflammatory sites. Proc Natl Acad Sci U S A 2014;111:8173-8178.
13) Vanheule V, Boff D, Mortier A, Janssens R, Petri B, Kolaczkowska E, et al. CXCL9-derived peptides differentially inhibit neutrophil migration in vivo through interference with glycosaminoglycan interactions. Front Immunol 2017;8:530.
14) Vanheule V, Janssens R, Boff D, Kitic N, Berghmans N, Ronsse I, et al. The positively charged COOH-terminal glycosaminoglycan-binding CXCL9(74–103) peptide inhibits CXCL8-induced neutrophil extravasation and monosodium urate crystal-induced gout in mice. J Biol Chem 2015;290:21292-21304.
15) **Marques PE**, **Antunes MM**, David BA, Pereira RV, Teixeira MM, Menezes GB. Imaging liver biology in vivo using conventional confocal microscopy. Nat Protoc 2015;10:258-268.
16) Hinson JA, Roberts DW, James LP. Mechanisms of acetaminophen-induced liver necrosis. Handb Exp Pharmacol 2010;369-405.
17) Marques PE, Oliveira AG, Chang L, Paula-Neto HA, Menezes GB. Understanding liver immunology using intravital microscopy. J Hepatol 2015;63:733-742.
18) Adams DH, Ju C, Ramaiah SK, Uetrecht J, Jaeschke H. Mechanisms of immune-mediated liver injury. Toxicol Sci 2010;115:307-321.
19) Faust N, Varas F, Kelly LM, Heck S, Graf T. Insertion of enhanced green fluorescent protein into the lysozyme gene creates mice with green fluorescent granulocytes and macrophages. Blood 2000;96:719-726.
20) Lammermann T, Afonso PV, Angermann BR, Wang JM, Kastenmuller W, Parent CA, et al. Neutrophil swarms require LTB4 and integrins at sites of cell death in vivo. Nature 2013;498:371-375.
21) Liu ZX, Han D, Gunawan B, Kaplowitz N. Neutrophil depletion protects against murine acetaminophen hepatotoxicity. Hepatology 2006;43:1220-1230.
22) James LP, McCullough SS, Lamps LW, Hinson JA. Effect of N-acetylcysteine on acetaminophen toxicity in mice: relationship to reactive nitrogen and cytokine formation. Toxicol Sci 2003;75:458-467.
23) Lima BHF, Marques PE, Gomides LF, Mattos MS, Kraemer L, Queiroz-Junior CM, et al. Converging TLR9 and PI3Kgamma signaling induces sterile inflammation and organ damage. Sci Rep 2019;9:19085.
24) Dufourcq J, Neri W, Henry-Toulme N. Molecular assembling of DNA with amphipathic peptides. FEBS Lett 1998;421:7-11.
25) Mahoney DJ, Whittle JD, Milner CM, Clark SJ, Mulloy B, Buttle DJ, et al. A method for the non-covalent immobilization of heparin to surfaces. Anal Biochem 2004;330:123-129.
26) Lai JJ, Cruz FM, Rock KL. Immune sensing of cell death through recognition of histone sequences by C-type lectin-receptor-2d causes inflammation and tissue injury. Immunity 2020;52:123-135.e126.
27) Papayannopoulos V. Neutrophil extracellular traps in immunity and disease. Nat Rev Immunol 2018;18:134-147.
28) Fuchs TA, Brill A, Duerschmied D, Schatzberg D, Monestier M, Myers DD, et al. Extracellular DNA traps promote thrombosis. Proc Natl Acad Sci U S A 2010;107:15880-15885.
29) **Wang J**, **Hossain M**, Thanabalasuriar A, Gunzer M, Meininger C, Kubes P. Visualizing the function and fate of neutrophils in sterile injury and repair. Science 2017;358:111-116.
30) **Alvarenga D**, **Mattos M**, Lopes M, Marchesi S, Araújo A, Nakagaki B, et al. Paradoxical role of matrix metalloproteinases in liver injury and regeneration after sterile acute hepatic failure. Cells 2018;7:247.

31) Hogaboam CM, Bone-Larson CL, Steinhauser ML, Lukacs NW, Colletti LM, Simpson KJ, et al. Novel CXCR2-dependent liver regenerative qualities of ELR-containing CXC chemokines. FASEB J 1999;13:1565-1574.
32) Van Sweringen HL, Sakai N, Tevar AD, Burns JM, Edwards MJ, Lentsch AB. CXC chemokine signaling in the liver: impact on repair and regeneration. Hepatology 2011;54:1445-1453.
33) **Di Domizio J**, **Belkhodja C**, Chenuet P, Fries A, Murray T, Mondéjar PM, et al. The commensal skin microbiota triggers type I IFN-dependent innate repair responses in injured skin. Nat Immunol 2020;21:1034-1045.

Author names in bold designate shared co-first authorship.

Supporting Information

Additional Supporting Information may be found at onlinelibrary.wiley.com/doi/10.1002/hep4.1759/suppinfo.